

光学学报

1550 nm 高功率基横模半导体激光器及温度特性

常津源^{1,2}, 熊聪^{1*}, 祁琼¹, 王翠鸾¹, 朱凌妮¹, 潘智鹏^{1,2}, 王振诺^{1,2}, 刘素平¹, 马晓宇¹

¹中国科学院半导体研究所光电子器件国家工程中心, 北京 100083;

²中国科学院大学材料科学与光电技术学院, 北京 100049

摘要 通过引入渐变 Al 组分和脊型波导的设计, 制备了 1550 nm 高功率 AlGaInAs/InP 基横模半导体激光器, 室温连续工作模式下器件的斜率效率达到 0.35 mW/mA, 在 500 mA 的工作电流下, 输出功率为 138 mW, 垂直和水平方向的远场发散角分别为 32.9° 和 11.1°, 证明器件具有良好的基横模输出特性。同时, 建立高阶模截止条件温度模型, 研究了器件在不同温度下功率-电流(P - I)曲线中 kink 效应与远场发散角 steering 效应的产生原因, 阐述了温度对基横模和高阶模增益的影响机制。通过比较不同腔长器件发生 kink 效应的电流大小, 证明长腔长结构可以有效防止 kink 效应的发生。

关键词 激光器; 1550 nm; 基横模; kink 效应; 温度

中图分类号 TN248.4 文献标志码 A

DOI: 10.3788/AOS221772

1 引言

基横模半导体激光器由于具有较好的光束质量, 被广泛应用在光通信、光存储等领域。随着传输距离的增加和系统性能的提升, 对基横模激光器的输出功率和热稳定性的要求不断提高。研究者们相继提出了大光腔(LOC)^[1]、非对称窄波导(NAW)^[2]、平板耦合波导(SCOW)^[3]、极不对称大光腔(ETAS)^[4]等结构, 使目前基横模单管激光器的功率达到了 10 W 量级, 并且不断向低阈值、高光束质量、低发散角的趋势发展。随着激光器外延材料生长技术的不断成熟, 波长覆盖范围越来越宽, 其中 1550 nm 由于是人眼安全波段并且处于石英光纤第 3 个低吸收窗口, 是理想的远距离光纤传输波长, 被广泛应用于光纤通信、光谱分析、光电检测、医疗美容等领域。早期的 1550 nm 基横模激光器有源区材料以 InGaAsP 为主, 而 InGaAsP 具有较低的带阶比, 逐渐被温度性能更好的 AlGaInAs 代替, 但基于 AlGaInAs 的 1550 nm 基横模激光器输出功率与转换效率的整体水平仍然明显低于短波长基横模半导体激光器^[1, 5-7]。2019 年, 熊迪等^[8]设计了 AlGaInAs/InP 小发散角半导体激光器, 该激光器在 200 mA 电流下输出功率不足 35 mW。同年王皓等^[9]提出了 1550 nm 高速直调分布式反馈(DFB)激光器阵列, 其单通道输出功率最大可达 160 mW。目前相关研究中存在的普遍问题是器件的效率较低、输出功率不高, 而且针对器件可靠性和温

度特性的研究较少。随着注入电流的增加, 基横模半导体激光器的功率-电流(P - I)曲线会产生明显的 kink 效应, 伴随出现远场中心的侧向偏移并产生 steering 效应, 导致激光器的最大输出功率受到限制, 器件的光束质量和单模光纤的耦合效率显著降低。关于产生 kink 效应的原因, Lang^[10]总结出 3 个因素, 即烧孔效应(SHB)、折射率关于载流子密度的负相关性、波导侧向不对称性; Ten Cate 等^[11]归结为由自由载流子吸收造成的自热效应。为提高发生 kink 效应的阈值功率, 研究人员相继提出采用反波导限制层脊型结构^[12]、脊型两侧引入高电阻区^[13]、降低二氧化硅绝缘层厚度^[14]等方法。此外, 在外延层中引入 p 型重掺杂^[15-16]和非对称波导^[17]也被证明对于抑制 kink 效应具有积极作用。

本文设计并制备了 1550 nm 高功率 AlGaInAs/InP 基横模激光器, 通过对功率曲线、远场分布、内量子效率和损耗等相关参数的测量, 建立了高阶模截止条件的温度模型, 结合实验分析了 kink 效应和 steering 效应产生的原因, 同时证明采用长腔长结构更有助于防止 kink 效应的产生。

2 器件制备

采用低压金属有机物化学气相沉积(LP-MOCVD)外延生长系统进行材料生长, 在 n-InP 衬底上依次生长 2000 nm 的 InP 下包层, 200 nm 的 AlGaInAs n 型下波导, 由 10 nm 厚、1% 张应变的

收稿日期: 2022-09-30; 修回日期: 2022-10-25; 录用日期: 2022-10-31; 网络首发日期: 2022-11-04

基金项目: 中国科学院战略性先导科技专项(B类)(XDB43030301)

通信作者: *xiongcong@semi.ac.cn

AlGaInAs量子垒和7 nm厚的AlGaInAs量子阱组成的多量子阱结构,200 nm的AlGaInAs p型上波导,2400 nm的InP上包层以及170 nm的InGaAs欧姆接触层。波导层AlGaInAs材料中Al的原子数分数呈渐变形式,变化范围为0.31~0.35,越靠近有源区Al的原子数分数越低,该设计可以有效降低高功率输出时有源区附近Al的氧化速率^[7],提高器件可靠性。同时,随着Al原子数分数的增加,AlGaInAs折射率逐渐降低^[18],使得整个器件的限制因子和远场发散角减小,器件的饱和功率增大。

在得到合格的外延片之后对基横模器件脊型结构参数进行计算。一阶模截止时台面宽度^[19]的计算公式为

$$\omega = \frac{\lambda_0}{2\sqrt{n_{\text{eff}2}^2 - n_{\text{eff}1}^2}}, \quad (1)$$

式中: ω 为脊型台面宽度; λ_0 为波长; $n_{\text{eff}2}$ 和 $n_{\text{eff}1}$ 分别为脊型区和脊型区两侧波导的有效折射率。根据有效折射率法,垂直于外延生长方向的 $n_{\text{eff}1}$ 与刻蚀剩余厚度有关。当刻蚀深度过大时,需要更小的脊型宽度才能实现基横模输出;当刻蚀深度过小时,电流扩散速度加快,导致器件的内外量子效率降低^[20]。为了制备合格的脊型结构,采用SiO₂和光刻胶同时作为掩模,利用电感耦合等离子体(ICP)干法刻蚀,以CH₄、Cl₂和Ar为刻蚀气体制出脊型结构,最终制备器件的台面宽度为5.4 μm、刻蚀深度为2 μm,此结构模拟的光场分布如图1所示。

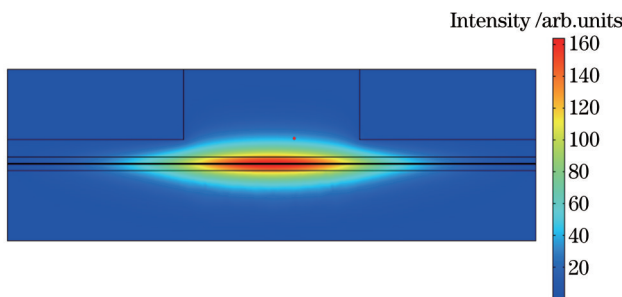


图1 脊型结构的光场分布

Fig. 1 Light field distribution of ridge structure

干法刻蚀后,在外延片p面采用等离子体增强化学气相沉积(PECVD)方法生长约200 nm厚的SiO₂介质膜作为绝缘层,经过光刻和湿法腐蚀形成电流注入窗口,通过磁控溅射方法制作p面TiPtAu电极;经减薄抛光后,真空蒸镀n面AuGeNi电极,并进行快速热退火处理。处理结束后将大片材料解理成不同腔长的巴条进行端面镀膜(抗反射率和高反射率分别为7%和98%),将镀膜后的巴条解理成管芯,并按p面向上封装在COS热沉中。封装之前管芯结构的扫描电子显微镜(SEM)图像如图2所示。

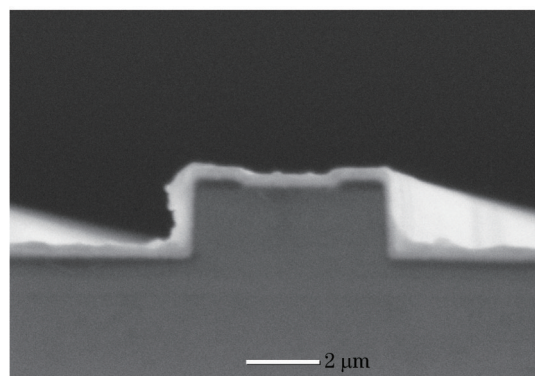


图2 AlGaInAs/InP半导体激光器管芯结构SEM图像

Fig. 2 SEM image of AlGaInAs/InP semiconductor laser die structure

3 器件性能测试

将腔长为1000 μm的单管器件放置在带有半导体制冷器(TEC)控温系统的激光器综合测试仪上进行性能测试,室温下(24 °C)连续工作模式(CW)器件的功率(P)-电流(I)-电压(V)曲线如图3所示。

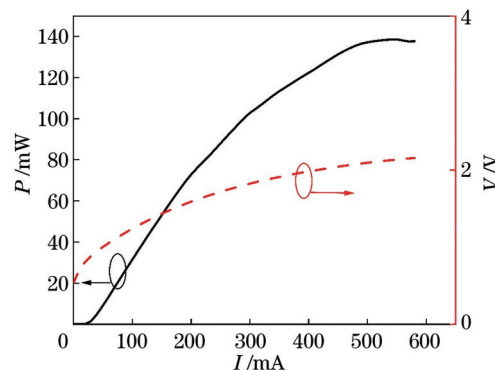


图3 室温下器件 P - I - V 曲线

Fig. 3 P - I - V curves of device at room temperature

器件的阈值电流为29 mA,斜率效率最大达到0.35 mW/mA,当电流达到500 mA时趋于热饱和,最大输出功率为138 mW。在器件最高输出功率下,测得的远场特性如图4所示。可以看到,器件在水平和垂直方向的光场呈现明显的高斯分布特征,没有高阶模旁瓣,证明该器件具有良好的基横模特性。垂直于外延生长方向1/2最大能量处的发散角为32.9°,平行于外延生长方向1/2最大能量处的发散角为11.1°。

分别制备腔长为1000、2000、3000、4000 μm的单管器件,并在室温下进行测试比较,根据式(2),可将外微分量子效率对腔长进行拟合,得到

$$\frac{1}{\eta_d} = \frac{1}{\eta_i} \left[1 + 2\alpha_i L / \ln \left(\frac{1}{R_b R_f} \right) \right], \quad (2)$$

式中: η_d 为外微分量子效率; η_i 为内量子效率; α_i 为内损耗; L 为腔长; R_b 和 R_f 分别为背光面和出光面的反

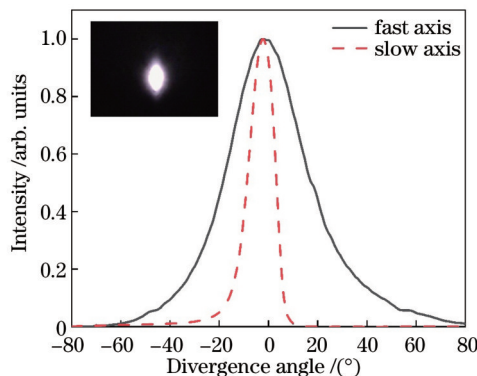


图4 最高功率输出下器件远场光斑与发散角

Fig. 4 Far-field beam spot and divergence angle of the device at the highest power output

射率。从图5所示的拟合结果得到内量子效率 $\eta_i=53.6\%$ 、内损耗 $\alpha_i=6.24\text{ cm}^{-1}$ 。

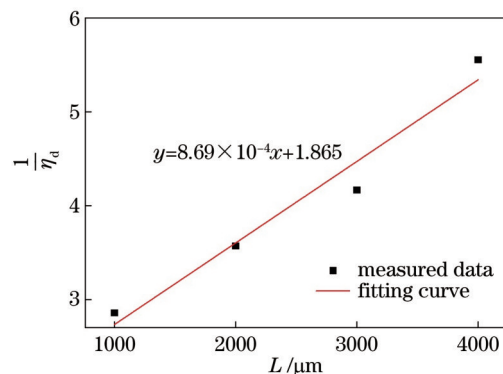
图5 外微分量子效率 $1/\eta_d$ 与腔长 L 的关系曲线

Fig. 5 Curve of external differential quantum efficiency $1/\eta_d$ versus cavity length L

4 器件温度特性分析

调节TEC温度,使器件在不同温度下工作并测试其性能参数,图6所示为不同温度下器件的P-I曲线。从图6可以看出,当温度从10℃上升至97℃时,阈值

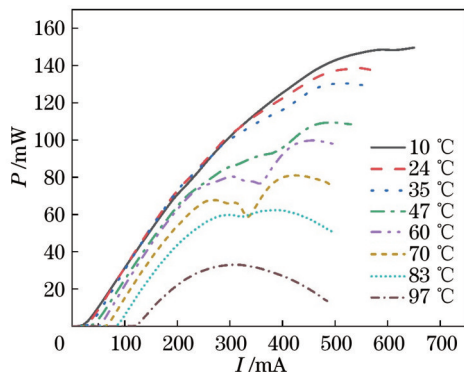


图6 不同温度下器件功率-电流曲线

Fig. 6 Power versus current curves of devices at different temperatures

电流从23.7 mA增大至121.1 mA,斜率效率从最大值0.36 mW/mA降低至0.23 mW/mA,饱和电流从500 mA降低至不足300 mA,饱和功率从峰值——10℃时的150 mW下降到97℃时的33 mW,下降了80%。升温导致器件性能出现大幅降低,是因为高温下费米占有概率函数的展宽使得注入的载流子处于更广的能量范围,从而使得增益谱变平、展宽^[21],此时为满足阈值条件,需要将更多载流子注入有源区,而非掺杂有源区中高浓度载流子又会带来更大的自由载流子吸收损耗(FCA)^[22]和俄歇复合损耗^[23]。高温下载流子泄漏增加,从而降低了内量子效率;泄漏的载流子积累在波导层,也会影响波导层以外的FCA^[24]。最终器件总损耗增加,使得高温下器件出现阈值电流增加、斜率效率降低、饱和电流减小、热饱和功率降低等现象。

半导体激光器阈值电流与温度的关系^[25]为

$$I_{\text{th}}(T) = I_{\text{th}}(T_r) \exp\left(\frac{T - T_r}{T_0}\right), \quad (3)$$

式中: T 为温度; $I_{\text{th}}(T)$ 为不同温度下的阈值电流; T_r 为室温; $I_{\text{th}}(T_r)$ 为室温下的阈值电流; T_0 为特征温度。将式(3)进行变形和拟合,可以得到器件的特征温度。如图7所示,器件的特征温度为12℃。

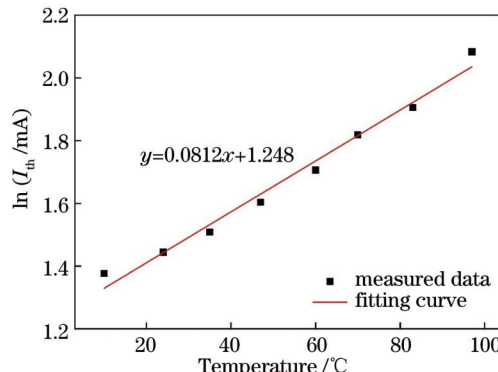


图7 阈值电流随温度的变化曲线

Fig. 7 Curve of threshold current versus temperature

从图6还可以发现,随着温度的升高,P-I曲线愈发无法保持为圆滑曲线。当温度升高至35℃时,曲线出现明显扭折;温度继续增加,发生扭折处的电流逐渐减小,当温度达到70℃时扭折程度达到最大;当温度继续上升时,扭折程度降低,直至升温至97℃,扭折完全消失。P-I曲线的这种扭折现象即是kink效应。

为研究kink效应的产生原因,建立了器件波导结构高阶模截止温度模型^[26]。下面定义各层波导折射率与温度的关系,即

$$n_{\text{layer}}(T) = n_{\text{layer}} + (T - T_r) \frac{dn}{dT}, \quad (4)$$

式中: $n_{\text{layer}}(T)$ 为不同温度下各层材料的折射率; n_{layer} 为常温下各层材料的折射率; $\frac{dn}{dT}$ 为折射率随温度的变化率。在建立模型时作出如下假设:1)忽略不同温度

时波长漂移对折射率的色散。2)忽略载流子注入对折射率的影响。前文已经提到载流子注入区域主要为有源区,绝大部分光场占据的波导层一般为低掺杂甚至非故意掺杂,因此其对折射率的影响非常小^[27]。对于有源区,尽管载流子注入会降低材料的折射率,使材料出现反波导现象,然而器件在高输入功率下工作时有源区温度较高,这在一定程度上削弱了载流子带来的影响。实际上随着电流的增加,器件垂直方向的远场发散角并不会发生较大变化^[7, 28]。3)严格意义上 $\frac{dn}{dT}$ 与波长以及各层材料组分有关,但由于相关研究还不完善,故 $\frac{dn}{dT}$ 取常数 $1.9 \times 10^{-4} \text{ }^{\circ}\text{C}^{-1}$ ^[26]。由式(1)、(4)可以得出在不同温度下,一阶模截止时脊波导包层刻蚀剩余厚度与脊宽的关系,如图8所示。

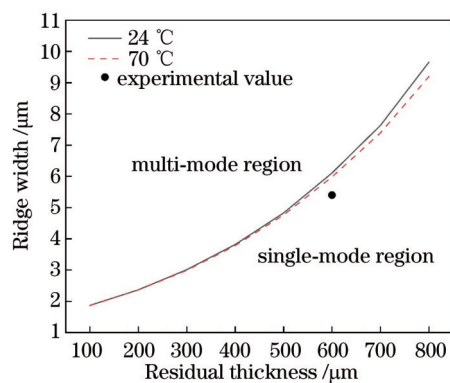


图8 不同温度下一阶模截止时包层剩余厚度与脊宽的关系曲线

Fig. 8 Curves of residual thickness of cladding versus ridge width at different temperatures when the first-order mode is cut off

由图8可知,在相同温度下,脊宽越大,一阶模截止时的包层刻蚀剩余厚度越大。当器件在常温下满足基模输出条件的脊宽与刻蚀剩余厚度确定时,温度的升高使截止条件曲线向更大的剩余厚度方向移动,愈发接近器件现有的剩余厚度,也就是说相比于常温,高温下器件单模输出条件更加苛刻,更容易引起高阶模谐振。当输入电流不断增大时,高阶模与基模发生模式竞争,同时SHB带来的增益峰峰值移动使得高阶模获得的增益增加,而基模获得的增益降低^[29],整体输出功率开始下降;随着高阶模增益逐渐稳定,电流继续增加,整体输出功率开始增加^[16],最终产生kink效应。然而,当温度增加到一定程度后,由于载流子损耗已经非常严重,器件的输出直接进入热饱和状态,这是在高温下kink效应消失的原因。

如图9所示,在60 °C温度的功率曲线中选取A、B、C 3个点,此时器件分别在200、340、445 mA电流下工作,分别表示器件产生kink效应的前后状态,3个点在平行于外延方向的远场发散角分别为8.6°、9.6°、

10.4°。出现这种发散角逐渐增加的现象是因为高温下截止曲线的移动等效于刻蚀深度增加,从而导致侧向折射率差增大;同时,高功率输出下载流子的大量消耗使得脊波导中心处有源区折射率增大,形成自聚焦效应,导致远场发散角增大^[30]。从图9还可以观察到,远场发散角的峰在产生kink效应前后发生明显的偏移,最大偏移角度为2.2°,这种现象即为steering效应,这是由空间烧孔造成的载流子侧向不均匀分布导致的^[29]。

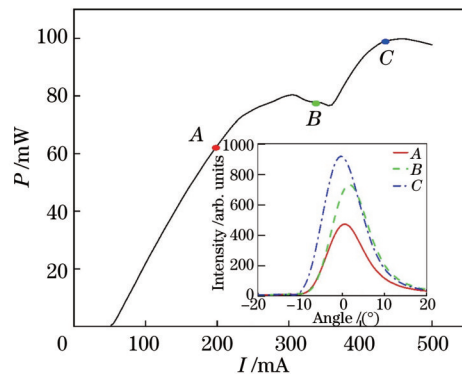


图9 60 °C时的P-I曲线,插图为水平方向远场发散角随电流的变化

Fig. 9 P-I curve at 60 °C, the inset shows the variation of horizontal far-field divergence angle with current

研究了1550 nm基横模激光器在不同腔长下的kink效应,如图10所示,当温度为60 °C时,具有不同腔长的器件产生kink效应时的电流大小并不相同,且腔长越长,产生kink效应时的电流越大,这是因为在式(4)中采用的模型忽略了器件自身由于欧姆接触产生的焦耳热,将热沉温度作为器件本身的温度。实际上需要考虑器件本身的发热以及器件和热沉之间的热传导,器件腔长越长,表征器件传热性能的热阻越小,器件导热性能就越好,这使得器件可以在不产生kink效应的条件下加载更高的工作电流。由图10可以得出,采用长腔长可以抑制kink效应的产生^[31]。然而,结合

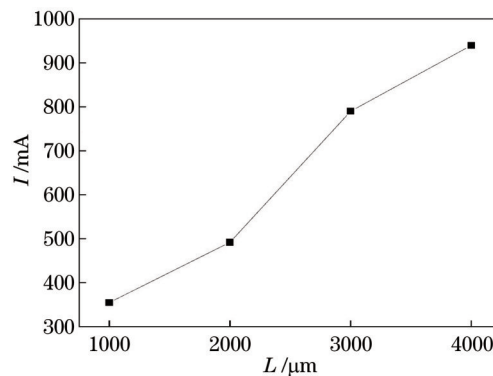


图10 具有不同腔长L的器件产生kink效应时的电流值
Fig. 10 Current at which the kink effect occurs in devices with different cavity lengths

图5和图10可以看出,腔长越长,器件外微分量子效率越低,故需要根据器件实际情况以及最终需求对腔长进行优化。

5 结 论

设计并制备了1550 nm高功率基横模AlGaInAs/InP激光器,该器件在室温下获得了0.35 mW/mA的斜率效率与138 mW的功率输出,垂直方向和水平方向的远场发散角分别为32.9°和11.1°,表现出良好的基横模特性。通过对高温下器件P-I曲线中kink效应的分析,利用波导折射率与温度的关系,建立了高阶模截止温度模型,证明热量可以改变折射率,进而影响高阶模截止条件,导致基横模增益降低,使得器件产生kink效应,同时,由空间烧孔等效应造成的载流子分布不均匀使得远场发散角产生steering效应。通过比较不同腔长器件产生kink效应的电流大小,证明长腔长器件可以有效防止kink效应的产生。

参 考 文 献

- [1] 曼玉选,仲莉,马晓宇,等.极低内部光学损耗975 nm半导体激光器[J].光学学报,2020,40(19): 1914001.
Man Y X, Zhong L, Ma X Y, et al. 975 nm semiconductor lasers with ultra-low internal optical loss[J]. Acta Optica Sinica, 2020, 40(19): 1914001.
- [2] Ryvkin B S, Avrutin E A. Nonbroadened asymmetric waveguide diode lasers promise much narrower far fields than broadened symmetric waveguide ones[J]. Journal of Applied Physics, 2005, 98(2): 026107.
- [3] Plant J J, Jucodawlkis P W, Huang R K, et al. 1.5- μ m InGaAsP-InP slab-coupled optical waveguide lasers[J]. IEEE Photonics Technology Letters, 2005, 17(4): 735-737.
- [4] Kaul T, Erbert G, Maassdorf A, et al. Extreme triple asymmetric (ETAS) epitaxial designs for increased efficiency at high powers in 9xx-nm diode lasers[J]. Proceedings of SPIE, 2018, 10514: 105140A.
- [5] Hu C W, Lee F M, Huang K F, et al. Linear GRINSCH 1.55- μ m InGaAsP/InP strained multiple quantum well laser diodes grown by substrate temperature control[J]. Journal of the Electrochemical Society, 2006, 153(4): G309.
- [6] Menna R, Komissarov A, Maiorov M, et al. High power 1550 nm distributed feedback lasers with 440 mW CW output power for telecommunication applications[C]//Technical Digest. Summaries of papers presented at the Conference on Lasers and Electro-Optics, May 11, 2001, Baltimore, MD, USA. New York: IEEE Press, 2001: CPD12-CP1.
- [7] 柯青.1.55 μ m InP基大功率半导体DFB激光器的研究[D].北京:中国科学院大学,2015.
Ke Q. Study on 1.55 μ m InP-based high power semiconductor DFB laser[D]. Beijing: University of Chinese Academy of Sciences, 2015.
- [8] 熊迪,郭文涛,郭小峰,等.1.55 μ m AlGaInAs/InP小发散角量子阱激光器的仿真和制备[J].红外与毫米波学报,2019(4): 412-418.
Xiong D, Guo W T, Guo X F, et al. Simulation and fabrication of 1.55 μ m AlGaInAs/InP quantum well lasers with low beam divergence[J]. Journal of Infrared and Millimeter Waves, 2019 (4): 412-418.
- [9] 王皓,张瑞康,陆丹,等.1.55- μ m大功率高速直调半导体激光器阵列[J].光学学报,2019,39(9): 0914001.
Wang H, Zhang R K, Lu D, et al. 1.55- μ m high-power high-speed direct-modulated semiconductor laser array[J]. Acta Optica Sinica, 2019, 39(9): 0914001.
- [10] Lang R. Lateral transverse mode instability and its stabilization in stripe geometry injection lasers[J]. IEEE Journal of Quantum Electronics, 1979, 15(8): 718-726.
- [11] Ten Cate J W R, Weegels L M, van Bakel A H, et al. Kinks induced by free-carrier absorption in weakly index guided semiconductor lasers[J]. Applied Physics Letters, 1997, 71(1): 19-21.
- [12] Takada H, Numai T. Ridge-type semiconductor lasers with antiguide cladding layers for horizontal transverse modes[J]. IEEE Journal of Quantum Electron, 2009, 45(8): 917-922.
- [13] Yuda M, Hirono T, Kozen A, et al. Improvement of kink-free output power by using highly resistive regions in both sides of the ridge stripe for 980-nm laser diodes[J]. IEEE Journal of Quantum Electronics, 2004, 40(9): 1203-1207.
- [14] Buda M, Tan H H, Fu L, et al. Improvement of the kink-free operation in ridge-waveguide laser diodes due to coupling of the optical field to the metal layers outside the ridge[J]. IEEE Photonics Technology Letters, 2003, 15(12): 1686-1688.
- [15] Miyashita M, Nakayama T, Takase T, et al. High-power red laser mode for recordable DVDs[J]. Proceedings of SPIE, 2004, 5365: 148-154.
- [16] 邹德恕,廉鹏,徐晨,等.量子阱半导体激光器P-I特性曲线扭折的研究[J].光电子·激光,2002,13(6): 547-549.
Zou D S, Lian P, Xu C, et al. Study on kinks in P-I characteristic curves of semiconductor quantum-well stripe geometry lasers[J]. Journal of Optoelectronics·Laser, 2002, 13 (6): 547-549.
- [17] Shigihara K, Kawasaki K, Yamamura S, et al. High-power and highly reliable 1020-nm ridge waveguide laser diodes with small aspect ratio as a pumping source for praseodymium-doped fiber amplifiers[J]. IEEE Photonics Technology Letters, 2003, 15(5): 640-642.
- [18] Ivanov A V, Kurnosov V D, Kurnosov K V, et al. Refractive indices of solid AlGaInAs solutions[J]. Quantum Electronics, 2007, 37(6): 545-548.
- [19] 张娜玲,井红旗,袁庆贺,等.高功率1060 nm锥形激光器[J].光学学报,2022,42(5): 0514002.
Zhang N L, Jing H Q, Yuan Q H, et al. High power 1060 nm tapered laser[J]. Acta Optica Sinica, 2022, 42(5): 0514002.
- [20] Wenzel H, Erbert G, Knauer A, et al. Influence of current spreading on the transparency current density of quantum-well lasers[J]. Semiconductor Science and Technology, 2000, 15(6): 557-560.
- [21] 拉里·A.科尔德伦,斯科特·W.科尔津.二极管激光器与集成光路[M].史寒星,译.北京:北京邮电大学出版社,2006.
Coldren L A, Corzin S W. Diode lasers and photonic integrated circuits[M]. Shi H X, Transl. Beijing: Beijing University of Posts and Telecommunications Press, 2006.
- [22] Pikhtin N A, Slipchenko S O, Sokolova Z N, et al. Internal optical loss in semiconductor lasers[J]. Semiconductors, 2004, 38(3): 360-367.
- [23] Yoshida Y, Watanabe H, Shibata K, et al. Analysis of characteristic temperature for InGaAsP BH lasers with p-n-p-n blocking layers using two-dimensional device simulator[J]. IEEE Journal of Quantum Electronics, 1998, 34(7): 1257-1262.
- [24] Ryvkin B, Avrutin E. Heating-induced carrier accumulation in the optical confinement layer and the output power in broadened symmetric and narrow asymmetric waveguide laser diodes[J]. Journal of Applied Physics, 2007, 101(12): 123115.
- [25] 张彦鑫,王警卫,吴迪,等.一种新型大功率单发射腔半导体激光器及其特性[J].中国激光,2010,37(5): 1186-1191.
Zhang Y X, Wang J W, Wu D, et al. A new package structure for high power single emitter semiconductor laser and performance analysis[J]. Chinese Journal of Lasers, 2010, 37(5): 1186-1191.

- [26] Tan W K, Wong H Y, Kelly A E, et al. Temperature behaviour of pulse repetition frequency in passively mode-locked InGaAsP/InP laser diode: experimental results and simple model [J]. IEEE Journal of Selected Topics in Quantum Electronics, 2007, 13(5): 1209-1214.
- [27] Chusseau L, Martin P, Brasseur C, et al. Carrier-induced change due to doping in refractive index of InP: measurements at 1.3 and 1.5 μm [J]. Applied Physics Letters, 1996, 69(20): 3054-3056.
- [28] Horie H, Arai N, Mitsuishi Y, et al. Greater than 500-mW CW kink-free single transverse-mode operation of weakly index guided buried-stripe type 980-nm laser diodes[J]. IEEE Photonics Technology Letters, 2000, 12(10): 1304-1306.
- [29] Guthrie J, Tan G L, Ohkubo M, et al. Beam instability in 980-nm power lasers: experiment and analysis[J]. IEEE Photonics Technology Letters, 1994, 6(12): 1409-1411.
- [30] 刘储. 脊型波导852 nm半导体激光器模式特性研究[D]. 北京: 北京工业大学, 2017.
- [31] Liu C. Fundamental lateral mode characteristics of the 852 nm ridge waveguide semiconductor laser diode[D]. Beijing: Beijing University of Technology, 2017.
- [31] Yagi T, Nishiguchi H, Yoshida Y, et al. High-power, high-efficiency 660-nm laser diodes for DVD-R/RW[J]. IEEE Journal of Selected Topics Quantum Electronics, 2003, 9(5): 1260-1264.

1550 nm High-Power Fundamental Transverse Mode Semiconductor Laser and Its Temperature Characteristics

Chang Jinyuan^{1,2}, Xiong Cong^{1*}, Qi Qiong¹, Wang Cuiluan¹, Zhu Lingni¹, Pan Zhipeng^{1,2},
Wang Zhennuo^{1,2}, Liu Suping¹, Ma Xiaoyu¹

¹National Engineering Research Center for Optoelectronic Devices, Institute of Semiconductors, Chinese Academy of Sciences, Beijing 100083, China;

²College of Materials Science and Optoelectronic Technology, University of Chinese Academy of Sciences, Beijing 100049, China

Objective 1550 nm transverse mode semiconductor laser has been applied in many fields such as optical fiber communication, spectral analysis, photoelectric detection, medical cosmetology. At the same time, it is also the research basis of communication band semiconductor optical amplifiers and narrow linewidth transverse mode semiconductor lasers. The kink effect refers to the fact that the *P-I* curve of the fundamental transverse mode device will be bent, which will greatly reduce the output power of lasers. At the same time, the steering effect will cause the far-field divergence angle of the horizontal direction of the device to shift and reduce the beam quality of the fundamental transverse mode device. For the 1550 nm semiconductor laser in the communication band, it will affect the efficiency of coupling with the single-mode fiber. In this paper, a 1550 nm high-power AlGaInAs/InP-based transverse mode semiconductor laser is designed and fabricated, and the kink effect is studied.

Methods In this paper, a gradual Al component is introduced into the waveguide, and the atomic number fraction is 0.31–0.35. In addition, the atomic number fraction of Al component becomes lower when getting closer to the active region. This design can effectively reduce the oxidation of Al near the active region at the high-power output and improve the reliability of the device. At the same time, with the gradual increase in the Al atomic number fraction, the refractive index of AlGaInAs decreases gradually, which reduces the confinement factor of the whole device, improves the saturation power of the device, and lowers the far-field divergence angle. In order to realize the fundamental transverse mode output, the relationship between the residual thickness of cladding and ridge width is calculated according to the effective refractive index method. In view of the actual process, the final ridge width is 5.4 μm , and the etching depth is 2 μm (Fig. 2). In order to analyze the kink effect occurring after device fabrication, a temperature model with high-order mode cutoff is established (Fig. 8). The mode output characteristics of the device before and after temperature rise are analyzed, and the influence of temperature on the kink effect is proved by measuring devices with different cavity lengths (Fig. 10).

Results and Discussions The threshold current of the device designed and fabricated in this paper is 29 mA, the maximum slope efficiency is 0.35 mW/mA, and the maximum output power is 138 mW (Fig. 3). At the highest output power of the device, the vertical and horizontal divergence angles are 32.9° and 11.1°, respectively (Fig. 4), which proves that the device has good fundamental transverse mode output characteristics, and the internal quantum efficiency and loss are 53.6% and 6.24 cm^{-1} , respectively (Fig. 5). The *P-I* curve of the device at different operating temperatures is observed (Fig. 6). The current increasing curve tends to be flat at the same temperature, which is caused by the broadening and reduction of the gain spectrum due to the increase in the current and the saturation state of the device due to a large amount of carrier leakage. For the *P-I* folding phenomenon at a high temperature, according to the temperature model of the higher-order mode cut-off,

it is believed that the temperature rise is more likely to make the higher-order mode compete with the fundamental transverse mode generation mode. Furthermore, as the gain of the higher-order mode increases, the gain of the fundamental transverse mode decreases, which leads to the kink effect. With the kink effect, the far-field divergence angle also has a steering effect. The peak of the far-field divergence angle shifts by 2.2° (Fig. 9), which is caused by the non-uniform lateral distribution of charge carriers. For devices with different cavity lengths, a longer cavity length is often accompanied by a higher current value of the kink effect. As the long cavity length structure has better heat dissipation, it proves not only that the temperature affects the occurrence of the kink effect but also that the long cavity length structure can better suppress the kink effect.

Conclusions In this paper, a 1550 nm high-power AlGaInAs/InP laser with the transverse mode is designed and fabricated. The device achieves a slope efficiency of 0.35 mW/mA and a power output of 138 mW at room temperature. The vertical and horizontal far-field divergence angles are 32.9° and 11.1° , respectively. By analyzing the kink effect in the P - I curve of the device at a high temperature and using the relationship between the refractive index of the waveguide and the temperature, a temperature model of the high-order mode cutoff is established. It shows that the heat changes the refractive index and then affects the high-order mode cutoff condition, which leads to the reduction of the gain of the fundamental transverse mode and the occurrence of the kink effect in the device. The non-uniform carrier distribution caused by the effect of hole burning in space makes the far-field divergence angle show the steering effect. By comparing the current at which the kink effect occurs in devices with different cavity lengths, it is proved that the device with a long cavity length can effectively prevent the occurrence of the kink effect.

Key words lasers; 1550 nm; fundamental transverse mode; kink effect; temperature